Steps in CH_4 Oxidation on Pt and Rh Surfaces: High-Temperature Reactor Simulations

D. A. Hickman and L. D. Schmidt
Dept. of Chemical Engineering and Materials Science, University of Minnesota, Minneapolis, MN 55455

The direct oxidation of CH_4 to H_2 and CO in O_2 and in air at high temperatures over alumina foam monoliths coated with high loadings of Pt and Rh has been simulated using a 19-elementary-step model of adsorption, desorption and surface reaction steps with reaction parameters from the literature or from fits to previous experiments. The surface reaction model for Pt is in good agreement with previously reported low-pressure (0.1 to 1 torr) reactor measurements of CH_4 oxidation rates at temperatures from 600 to 1,500 K and of OH radical desorption during CH_4 oxidation at 1,300 to 1,600 K over polycrystalline Pt foils. The model predictions for both catalysts are also consistent with product selectivities observed over monolithic catalysts in an atmospheric-pressure laboratory-scale reactor, and the differences between Pt and Rh can be explained by comparing individual reaction steps on these surfaces. Because of the good agreement between the model and both low- and atmospheric-pressure reactor simulations, a complete energy diagram for methane oxidation at low coverages is proposed. The model results show that under CH_4-rich conditions at high temperatures, H_2 and CO are primary products of the direct oxidation of methane via a pyrolysis mechanism.

Introduction

The conversion of methane to liquid fuels is a problem that has generated much research in recent years. Two important routes for methane conversion to liquid fuels are methanol synthesis and the Fischer-Tropsch process. For both of these reaction systems, synthesis gas is generated in the first step and then converted to the final product in a second catalytic reactor.

Recently, Hickman and Schmidt (1992a, 1993) have demonstrated that the generation of synthesis gas by the *direct oxidation* of methane is a promising alternative to steam reforming. Surprisingly, high selectivities of H_2 and CO formation are achieved with almost complete conversion of the methane feed over Pt- and Rh-coated monolith catalysts at very short residence times. In addition, Rh catalysts have been shown to give hydrogen selectivities vastly superior to Pt catalysts.

Based on these recent atmospheric-pressure reactor studies and previous research on oxidation reactions over Pt and Rh, we have developed a 19-step surface reaction mechanism for the oxidation of CH_4 over Pt and Rh at high temperatures (>800 K) and low O_2 coverages. This mechanism combines previously published 12-step mechanisms for H_2 oxidation (Williams et al., 1992; Zum Mallen et al., 1993) with an additional seven steps which account for methane adsorption and the subsequent reversible oxidation and desorption steps. *Essentially all of the reaction rate parameters are from work previously reported in the literature.* The mechanism and notation are as follows:

$$\frac{m}{2}\,H_{2g} \underset{k_{dH}}{\overset{k_{aH}}{\rightleftarrows}} mH \qquad \text{(H)}$$

$$\frac{n}{2}\,O_{2g} \underset{k_{dO}}{\overset{k_{aO}}{\rightleftarrows}} nO \qquad \text{(O)}$$

$$H_2O_g \underset{k_{dW}}{\overset{k_{aW}}{\rightleftarrows}} H_2O \qquad \text{(W)}$$

$$CO_g \underset{k_{dCM}}{\overset{k_{aCM}}{\rightleftarrows}} CO \qquad \text{(CM)}$$

Correspondence concerning this article should be addressed to L. D. Schmidt.
Present address of D. A. Hickman: The Dow Chemical Company, Midland, MI 48674.

$$CO_{2g} \underset{k_{dCD}}{\overset{k_{aCD}}{\rightleftarrows}} CO + O \qquad \text{(CD)}$$

$$CH_{4g} \xrightarrow{k_{aM}} C + 4H \qquad \text{(M)}$$

for adsorption/desorption and

$$H + O \underset{k_{-1}}{\overset{k_1}{\rightleftarrows}} OH \qquad (1)$$

$$H + OH \underset{k_{-2}}{\overset{k_2}{\rightleftarrows}} H_2O \qquad (2)$$

$$2OH \underset{k_{-3}}{\overset{k_3}{\rightleftarrows}} H_2O + O \qquad (3)$$

$$C + O \underset{k_{-4}}{\overset{k_4}{\rightleftarrows}} CO \qquad (4)$$

for surface reactions. Note that for the purposes of this model, CH_4 and CO_2 chemisorption are each considered to be a one-step adsorption and dissociation, with CH_4 adsorption considered irreversible.

This mechanism was combined with a reactor model to simulate experiments at both low and atmospheric pressure reaction conditions. The following section will outline the equations and assumptions for all of the models discussed in this article.

Model

Surface species mass balances

In both the low-pressure and atmospheric pressure simulations, steady-state coverages of all species give the following expressions:

$$\frac{d\Theta_H}{dt} = 0 = k_{-1}\Theta_{OH}\Theta_{v,NC} - k_1\Theta_H\Theta_O - k_2\Theta_H\Theta_{OH} + k_{-2}\Theta_{H2O}\Theta_v + k_{aH}P_{H2}\Theta_v - k_{dH}\Theta_H + 4k_{aM}P_{CH4}\Theta_v \qquad (5)$$

$$\frac{d\Theta_O}{dt} = 0 = k_{-1}\Theta_{OH}\Theta_{v,NC} - k_1\Theta_H\Theta_O + k_3\Theta_{OH}^2\Theta_{v,NC} - k_{-3}\Theta_{H2O}\Theta_O\Theta_v + k_{aO}P_{O2}\Theta_{v,NC} - k_{dO}\Theta_O - k_4\Theta_C\Theta_O + k_{-4}\Theta_{CO}\Theta_{v,NC} + k_{aCD}P_{CO2}\Theta_v\Theta_{v,NC} - k_{dCD}\Theta_{CO}\Theta_O \qquad (6)$$

$$\frac{d\Theta_{OH}}{dt} = 0 = k_1\Theta_H\Theta_O - k_{-1}\Theta_{OH}\Theta_{v,NC} - k_2\Theta_H\Theta_{OH} + k_{-2}\Theta_{H2O}\Theta_v - 2k_3\Theta_{OH}^2\Theta_{v,NC} + 2k_{-3}\Theta_{H2O}\Theta_O\Theta_v \qquad (7)$$

$$\frac{d\Theta_C}{dt} = 0 = k_{-4}\Theta_{CO}\Theta_{v,NC} - k_4\Theta_C\Theta_O + k_{aM}P_{CH4}\Theta_v \qquad (8)$$

$$\frac{d\Theta_{CO}}{dt} = 0 = k_4\Theta_C\Theta_O - k_{-4}\Theta_{CO}\Theta_{v,NC} + k_{aCM}P_{CO}\Theta_v - k_{dCM}\Theta_{CO} + k_{aCD}P_{CO2}\Theta_v\Theta_{v,NC} - k_{dCD}\Theta_{CO}\Theta_O \qquad (9)$$

$$\frac{d\Theta_{H2O}}{dt} = 0 = k_2\Theta_H\Theta_{OH} - k_{-2}\Theta_{H2O}\Theta_v + k_3\Theta_{OH}^2\Theta_{v,NC} - k_{-3}\Theta_{H2O}\Theta_O\Theta_v + k_{aW}P_{H2O}\Theta_v - k_{dw}\Theta_{H2O} \qquad (10)$$

$$\Theta_v = 1 - \Theta_H - \Theta_{OH} - \Theta_C - \Theta_{CO} - \Theta_{H2O}. \qquad (11)$$

These equations include all 19 steps listed in the previous section, with $m = n = 1$ (first order O_2 and H_2 adsorption). We assumed that all species were adsorbed competitively, Eq. 11, except for oxygen. We assumed that oxygen was adsorbed noncompetitively with other species so that its effective fraction of vacant sites was $\Theta_{v,NC} = 1 - \Theta_O$. The results are not sensitive to the form of Θ_v because all coverages are $\ll 1$ except for Θ_O and Θ_C in most situations considered here. The details of site competition become very important at low temperatures, and more complex models will have to be developed for those situations.

Low-pressure CSTR

For simulations of the low-pressure CSTR experiments, the steady-state coverages, Eqs. 5–11, were solved simultaneously with six CSTR equations for the stable gas-phase species:

$$\frac{(P_i - P_{i,o})V_R N_{av}}{\tau A_{surf} R_g T_g N_0} = r_i \qquad (12)$$

(See the Notation section for definitions of variables used.) The seven steady-state coverage equations and six CSTR equations were solved simultaneously using the Newton-Raphson method with an analytical Jacobian matrix.

Atmospheric-pressure tubular reactor

Model Equations. For the atmospheric pressure reactor simulations, two different models were examined: plug flow tubular reactor (PFR) model with reactions on the tube walls and a one-dimensional tubular reactor model with mass transfer. The PFR model is the simpler of these two, which simultaneously integrates the species balances over the length of the tube

$$\frac{d(FP_i)}{dz} = \frac{\sigma F_0 R_g T_0}{A v_0 N_{av}} r_i. \qquad (13)$$

This equation is derived from a mass balance on species i over a differential length of the tube in the z-direction with the velocity (v) of the gases in this plug flow reactor allowed to vary as the total number of moles of gas changes due to reaction:

$$\frac{d(vc_i)}{dz} = \frac{\sigma}{N_{av}A} r_i \qquad (14)$$

The ratio σ/A is equivalent to the wall surface area per unit volume. Assuming ideal gases, the concentration is then converted to a partial pressure ($P_i = c_i R_g T_g$), and the velocity of the gases is proportional to the total molar flow rate and the gas temperature:

$$v = \frac{T_g F}{T_0 F_0} v_0. \tag{15}$$

Substituting this relationship into Eq. 14 and rearranging it gives the species balance in Eq. 13.

The total molar flow rate was assumed to vary in these simulations and was an additional variable in these calculations:

$$\frac{dF}{dz} = \frac{\sigma}{N_{av}} \sum_i r_i. \tag{16}$$

The PFR model simultaneously integrates Eqs. 13 and 16 while satisfying the algebraic surface coverage in Eqs. 5-11.

For the mass-transfer model, a mass-transfer coefficient was included to account for the transport of gas-phase species through the boundary layer near the catalyst surface. A mass-transfer coefficient based on a concentration driving force was used for these simulations:

$$k_c(c_i - c_{bi}) = \text{flux of } i \text{ from surface} \tag{17}$$

where the mass-transfer coefficient k_c is assumed to be constant over the length of the reactor. Because the adsorption rate parameters are based on species partial pressures, the concentrations were redefined in terms of the partial pressure in the bulk gas phase (P_{bi}) and the partial pressure near the surface (P_i):

$$\frac{k_c(P_i - P_{bi})}{R_g T_g / N_{av}} = r_i \tag{18}$$

The constant k_c was chosen to be based on a concentration driving force rather than a partial pressure driving force to be consistent with previous models of reactions in monoliths (Votruba et al., 1975; Young and Finlayson, 1976; Heck et al., 1976). Of course, a mass-transfer coefficient is merely an approximation to the real situation and is used in this work only to estimate the effect of interphase transport in these systems.

A gas-phase species balance on the reactor tube then gives the equation:

$$\frac{d(FP_i)}{dz} = \frac{\sigma k_c F_0}{A v_0} (P_i - P_{bi}). \tag{19}$$

Thus, the mass-transfer model simultaneously integrates Eqs. 16 and 19 while satisfying the algebraic Eqs. 5-11 and 18.

For both the PFR and mass-transfer models, a single uniform gas and catalyst temperature was assumed, with the autothermal reaction temperature a function of the heat generated by reaction and the heat lost through the reactor walls. The temperature can therefore be expressed as an integral balance over the reactor:

$$\Sigma F_{i0}\left(\Delta H^0_{f298} + \int_{298}^{T_0} C_p dT\right) - \Sigma F_i\left(\Delta H^0_{f298} + \int_{298}^{T} C_p dT\right) = (UA)_{\text{loss}}(T - 298) \tag{20}$$

where $(UA)_{\text{loss}}$ approximates the heat losses from the laboratory-scale reactor. Polynomial temperature-dependent expressions for molar heat capacities of the gas-phase species were used. This form of the energy balance equation was necessary because the autothermal temperatures measured in the experimental reactor were 50 to 100 K less than the adiabatic reaction temperature of the product gases. Since the reactor was insulated externally and radiation shields were placed before and after the catalytic monoliths in the reactor tube, radiative heat losses which are proportional to T^4 were neglected. The use of a single surface temperature in the model is a reasonable assumption, since the monolith catalysts in these experiments are well insulated and most of these very fast reactions occur at or near the front face of the monolith, where the temperature is very nearly uniform.

The solution algorithm thus involved integration of the mass-balance equations using Gear's method (Gear, 1971) while satisfying the appropriate algebraic equations. The autothermal temperature (T) for the product gases based on the input feed temperature (T_0) was compared to the estimate surface temperature (T_s), and a new T_s was estimated. Consecutive iterations, with new autothermal temperatures estimated by Newton's method, typically gave convergence to a solution within four or five iterations.

Model Parameters. In addition to the reaction rate parameters in Table 1, the model required estimation of the physical parameters in Eqs. 13-20, as shown in Table 2. The total molar flow rate is related to the channel dimensions and reactor pressure by assuming ideal gases:

$$F_0 = \frac{v_0 P A}{R_g T_0}. \tag{21}$$

In addition, $(UA)_{\text{loss}}$ was adjusted for a particular set of experiments to give autothermal temperatures close to those observed experimentally (typically about 100 K less than the adiabatic reaction temperature). Once estimated, this parameter was then kept constant for all simulations for a given set of experiments. For example, the same heat loss parameter was used for all model calculations in Figure 1.

For the atmospheric-pressure simulations, the same surface reaction rate parameters were used as in the low-pressure simulations with one modification. Unlike the low-pressure CSTR experiments where the gas is at ambient temperature ($T_g \sim 298$ K), the gases in these atmospheric pressure reaction simulations are assumed to be thermally accommodated (isothermal) with the catalyst surface ($T_s = T_g = T$). Thus, the adsorption coefficients k_{ai} were corrected for temperature in accordance with the kinetic theory relationship:

$$r_{\text{ads},i} = k_{ai} P_i = \frac{s_i(\Theta_v, T) P_i}{\sqrt{2\Pi M_i R_g T}}. \tag{22}$$

Comparison with Experiments

In this section, comparisons of model predictions with experimental results are presented. Low-pressure simulations for only Pt will be shown, since these experimental studies have only been performed with Pt. Simulations for atmospheric-pressure reactions over both Pt and Rh will then be compared with experimental results.

Table 1. Rate Parameters for Pt and Rh

Reaction		Platinum k ($torr^{-1}\cdot s^{-1}$)	Platinum E_a (kcal/mol)	Platinum Reference	Rhodium k ($torr^{-1}\cdot s^{-1}$)	Rhodium E_a (kcal/mol)	Rhodium References
$H+O\rightarrow OH$	(1)	1×10^{15}	2.5	Williams et al.	7×10^{12}	20	Wagner and Schmidt
$OH\rightarrow O+H$	(−1)	1×10^{8}	5	Williams et al.	1×10^{13}	5	Zum Mallen et al.
$H+OH\rightarrow H_2O$	(2)	9×10^{16}	15	Williams et al.	3×10^{17}	8	Zum Mallen et al.
$H_2O\rightarrow OH+H$	(−2)	1.8×10^{13}	37	Williams et al.	5×10^{14}	37	Zum Mallen et al.
$2OH\rightarrow H_2O+O$	(3)	1×10^{15}	12.3	Fisher and Gland	4×10^{15}	15	Zum Mallen et al.
$H_2O+O\rightarrow 2OH$	(−3)	~0	31	Thermodyn. constraints	~0	63	Thermodyn. constraints
$H_{2g}\rightarrow 2H$	(*a*H)	7.5×10^{4} ($s=0.05$)	0	Williams et al.	2.25×10^{5} ($s=0.16$)	0	Zum Mallen et al.
$2H\rightarrow H_{2g}$	(*d*H)	5×10^{12}	18	McCabe and Schmidt	5×10^{12}	18	Yates et al.
$O_{2g}\rightarrow 2O$	(*a*0)	1.25×10^{3} ($s=0.003$)	0	This work	3.5×10^{3} ($s=0.01$)	0	Oh et al. (1986)
$2O\rightarrow O_{2g}$	(*d*O)	5×10^{12}	52	Matsushima	5×10^{12}	70	Wagner and Schmidt Root et al.
$H_2O_g\rightarrow H_2O$	(*a*W)	5×10^{4} ($s=0.1$)	0	Williams et al.	7.4×10^{4} ($s=0.16$)	0	Zum Mallen et al.
$H_2O\rightarrow H_2O_g$	(*d*W)	1×10^{13}	10.8	Fisher and Gland	1×10^{13}	10.8	Kiss and Solymosi Wagner and Moylan
$OH\rightarrow OH_g$	(*d*OH)	1.5×10^{13}	48	Williams et al.	8.1×10^{11}	34	Zum Mallen et al.
$C+O\rightarrow CO$	(4)	5×10^{13}	15	This work	5×10^{13}	15	This work
$CO\rightarrow C+O$	(−4)	1×10^{11}	44	This work	1×10^{11}	40	This work
$CH_{4g}\rightarrow C+4H$	(*a*M)	5×10^{4}	10.3	Anderson and Maloney	3×10^{4}	5	Brass and Ehrlich
$CO_{2g}\rightarrow CO+O$	(*a*CD)	~0	36	Thermodyn. constraints	~0	26	Thermodyn. constraints
$CO+O\rightarrow CO_{2g}$	(*d*CD)	1×10^{15}	24	Campbell et al. (1980)	1×10^{12}	25	Brown and Sibener Campbell et al. (1979)
$CO_g\rightarrow CO$	(*a*CM)	3.21×10^{5} ($s=0.84$)	0	Campbell et al. (1981)	1.91×10^{5} ($s=0.5$)	0	Campbell et al. (1979)
$CO\rightarrow CO_g$	(*d*CM)	1×10^{13}	30	McCabe and Schmidt	4×10^{13}	31.6	Thiel et al.

CO and CO_2 generation from CH_4 and O_2 at low pressure over Pt

The kinetics of CH_4 oxidation over polycrystalline Pt have been measured previously at temperatures of 600 to 1,500 K for mixtures ranging in composition from 1/2 to 5/1 CH_4/O_2 at a total pressure of 0.1 to 10 torr (Hasenberg, 1985). Rates of H_2 and H_2O formation were not measured in those experiments. Figure 2 compares the predicted rates for CO and CO_2 generation with the experimentally measured rates. The reactor parameters for these experiments include a residence time (τ) of 0.25 s for all species, $V_R=600$ cm^3, and $A_{surf}=1.6$ cm^2.

As indicated in the figure, the model predicts the trends in r_{CO} and r_{CO2} reasonably well with the most accurate correlation between the model and experiments at high CH_4/O_2 ratios and temperatures. As the CH_4 pressure decreases, the model predicts a decrease in r_{CO} with lower temperatures that exceeds the experimentally observed decrease in the rate of CO generation. As will be discussed later, however, the rate parameters for both the CO oxidation reaction (CD) and CO desorption (CM) have been shown to change as the coverages of O or CO increase (Berlowitz et al., 1988; Campbell et al., 1980; Gland and Kollin, 1983; McCabe and Schmidt, 1977). For these simulations, literature values which apply in the low coverage limit have been used, and thus, the decreases in the temperature or CH_4/O_2 ratio give higher coverages of O and the model fails under these conditions. In additional simulations not shown here, decreasing the CO oxidation rate parameters to those in the literature for the high O coverage limit [$k_{dCD}=2\times10^{9}e^{11.7/RT}$ (Campbell

Table 2. Catalyst Parameters

Parameter	50 ppi Pt Foam	80 ppi Rh Foam
σ (cm)	0.20	0.12
A (cm^2)	2.5×10^{3}	9.0×10^{4}
v_o (cm/s) ($T_o=298$ K)	20.6	20.6
P (atm)	1.4	1.4

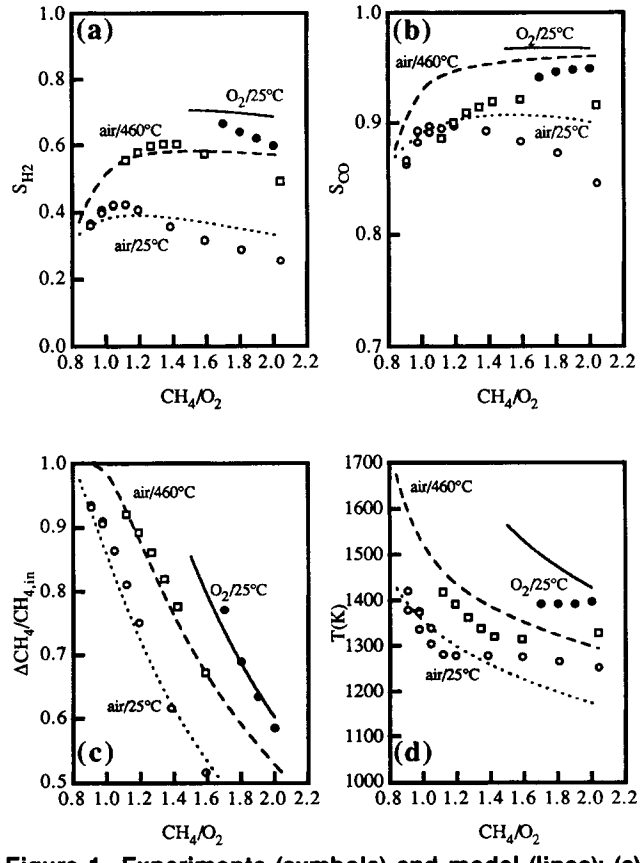

Figure 1. Experiments (symbols) and model (lines): (a) H_2 and (b) CO selectivities, (c) CH_4 conversions, and (d) surface temperatures for methane oxidation over a 50 ppi (pores per in.) Pt foam monolith with 11.6 wt. % Pt.

Open symbols and dashed lines represent CH_4-air feeds, closed symbols and solid lines represent CH_4-O_2 feeds, circles represent feed temperatures of 25°C and squares represent feeds preheated to 460°C.

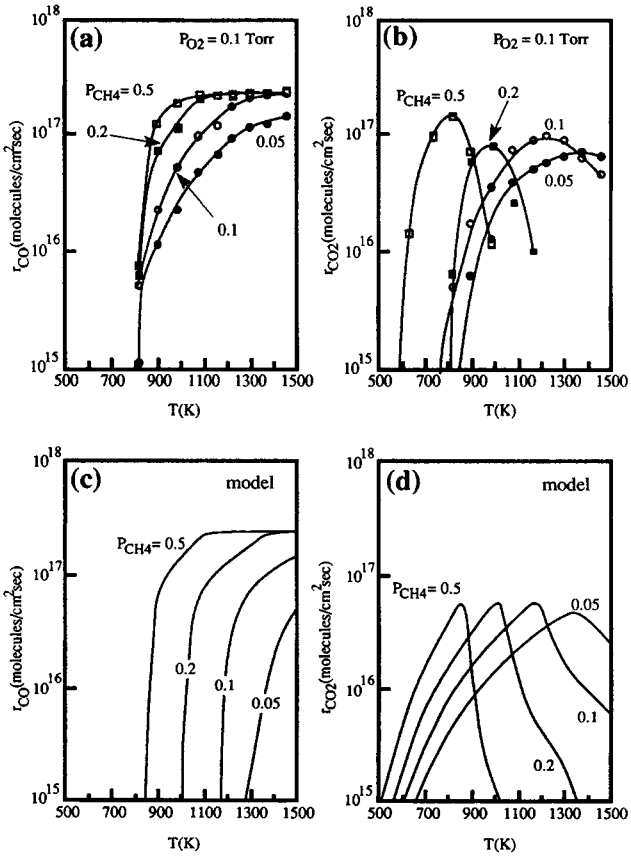

Figure 2. Experimentally measured (a) CO and (b) CO_2 generation rates during methane oxidation over a polycrystalline Pt foil vs. (c) CO and (d) CO_2 generation rates predicted by the low-pressure CSTR model ($P_{O2,o}$ = 0.1 torr).

The curves in (a) and (b) are *not* model fits.

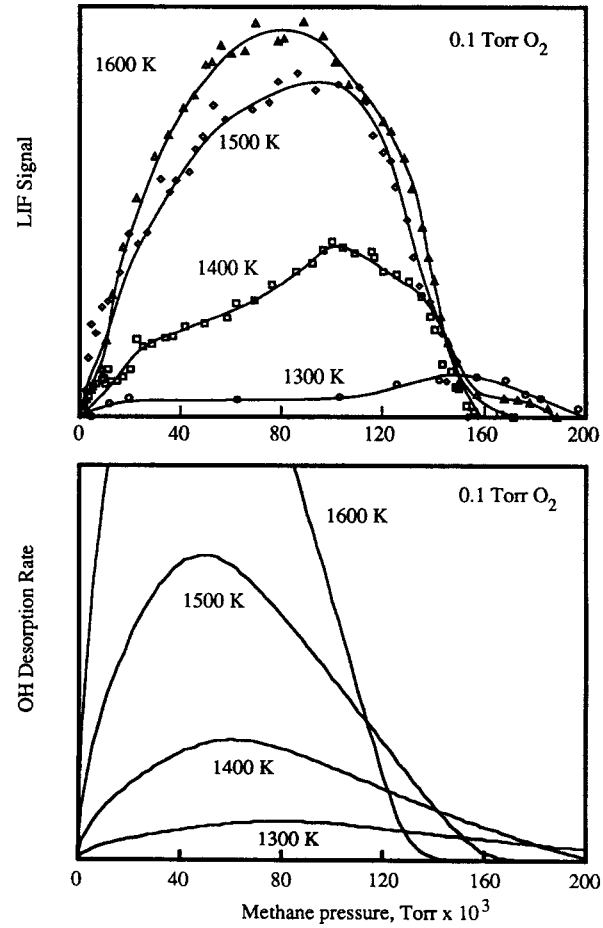

Figure 3. (a) Experimentally measured LIF signal (Marks and Schmidt, 1991) vs. (b) OH desorption flux from the surface predicted by the low-pressure CSTR model ($P_{O2,o}$ = 0.1 torr).

et al., 1980)] resulted in predicted CO rates in much better agreement with the experimental data at lower temperatures and lower CH_4 pressures. These parameters, however, did not give good correlations with the data in the high-temperature (low oxygen coverage) limit.

A final important point is that r_{CO} approaches an oxygen flux-limited value at high temperatures and high CH_4/O_2 ratios. Because the surface reaction model assumes that CH_4 adsorption is activated and reversible, Θ_C increases with temperature. To predict an O_2 flux limit consistent with the data, O_2 sticking must be independent of Θ_C. Hence, oxygen was assumed to be adsorbed noncompetitively on Pt. This assumption was also applied to Rh and has been used previously (Zum Mallen et al., 1993). In the low O coverage limit, besides giving the experimentally observed O_2 flux limit, this assumption has no additional effects on model predictions.

OH desorption rates from CH_4 and O_2 at low pressure over Pt

Previously reported (Marks and Schmidt, 1991) low-pressure studies of OH radical desorption during CH_4 oxidation on Pt foils at high temperatures (1,300 to 1,600 K) provide another test of the model predictions for the O-H reactions during CH_4 oxidation. In these experiments, reactions in Table 1 are assumed to occur, and OH_g is formed by the step $OH \rightarrow OH_g$, whose rate is negligible compared to those steps that produce major products. However, since the OH desorption rate is proportional to the OH surface coverage for a given surface temperature, laser induced fluorescence (LIF) experiments indirectly measure the surface coverage of this important reaction intermediate.

Figure 3 compares OH desorption rates (a) measured by LIF for various temperatures and compositions with (b) model predictions at the same conditions. Using previously published OH desorption rate parameters (Williams et al., 1992) with the additional term for OH desorption added to Eq. 7, the model gives good qualitative agreement with the experiments. The model predicts the maxima in OH desorption rates at CH_4/O_2 ratios only slightly smaller than observed in the LIF experiments. The model also gives a good approximation of the increase in OH desorption with temperature up to 1,500 K. The LIF experiments show that OH desorption becomes temperature-independent above ~1,500 K, suggesting a CH_4 flux limit, although the model does not predict this behavior. Making CH_4 adsorption (M) reversible might improve the agreement between model and experiment above 1,500 K, but since the atmospheric pressure studies generally had auto-

thermal temperatures below 1,500 K, this modification was not necessary.

Methane oxidation at atmospheric pressure over Pt: PFR model

In Figure 1, model predictions from the PFR model with Pt rate parameters are compared with experimental data for CH_4 oxidation with a Pt-coated foam monolith over a wide range of feed conditions. The model accurately predicts the large increase with autothermal reactor temperature in hydrogen selectivity, defined as:

$$S_{H2} = \frac{0.5F_{H2}}{F_{CH4in} - F_{CH4out}}, \tag{23}$$

and the accompanying improvement in fractional conversion of methane. Furthermore, the model predicts only a slight increase in selectivity of CO formation:

$$S_{CO} = \frac{F_{CO}}{F_{CH4in} - F_{CH4out}}. \tag{24}$$

The primary shortcoming of the model appears to be that it does not accurately predict the leveling off in autothermal reaction temperature at high CH_4/O_2 ratios and the accompanying decreases in S_{H2} and S_{CO}. This observed behavior is probably due to multilayer carbon deposits which are likely to occur for fuel-rich feeds and which are not included in the model. Thus, when the model predicts $\Theta_C \rightarrow 1$, the real system may deviate from the low coverage behavior assumed by the model.

The variation in species coverages predicted by the model can be seen in Figure 4, where coverages are plotted vs. axial position in the reactor tube. As shown in panel (a), even under the most lean conditions examined (15% CH_4 in air), carbon is the primary surface species, although all coverages are below 0.1 monolayers at the tube inlet, where most of the reaction occurs. As the reaction progresses and the O_2 is consumed, the carbon coverage increases as expected.

In Figure 4b (30% CH_4 in air), both the C and CO coverages exceed 0.1 monolayers very early in the reactor. Since the model does not account for multilayer carbon or changes in the reaction parameters due to adsorbate-adsorbate interactions, the model predictions deviate from the experimental data for feeds with CH_4/O_2 feed ratios close to 2/1.

Methane oxidation at atmospheric pressure over Rh: PFR model

Figures 5 and 6 show similar plots for results from the PFR model with Rh rate parameters compared to experimental data for CH_4 oxidation with a Rh-coated foam monolith. Again, the agreement between model and experiments is quite good at lower CH_4/O_2 ratios, with discrepancies occurring at higher CH_4/O_2 ratios. As with the Pt catalysts, the model appears to err when the coverages at the inlet approach unity.

The most important point to note is that the model accurately predicts the superiority of Rh over Pt for the production of H_2 and CO. An examination of the rate parameters reveals that the primary difference between Rh and Pt is the activation energy for OH formation, reaction 1. This and other differences in the energetics of the various surface reactions lead to remarkably different catalytic behaviors. A comparison of Figures 4 and 6 reveals some of the differences predicted by the model.

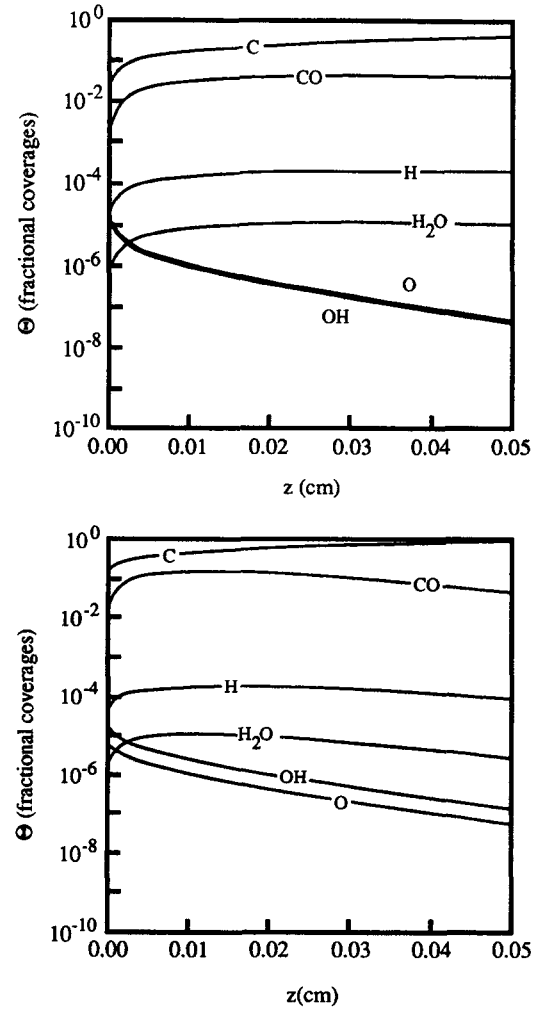

Figure 4. Fractional surface coverages as a function of axial position for PFR model simulations of room temperature feeds with (a) 15% CH_4 in air and (b) 30% CH_4 in air over a Pt catalyst.

One significant difference between Pt and Rh is the predicted oxygen coverage. For a room temperature feed of 15% CH_4 in air, Θ_O is less than $\sim 10^{-5}$ on Pt, while Θ_O is as high as 10^{-1} on Rh. Three factors contribute to higher Θ_O on Rh: (a) the autothermal reaction temperature is lower; (b) the sticking coefficient of oxygen is higher; and (c) the activation energy for oxygen desorption is higher. In spite of these higher O coverages, which would generally be expected to give better *total* oxidation selectivity, Rh is predicted to give better *partial* oxidation selectivities than Pt. This happens because Rh has an activation energy for OH formation of 20 kcal/mol vs. 2.5 kcal/mol for Pt and because Rh has a lower activation energy for CH_4 chemisorption.

Methane oxidation at atmospheric pressure over Pt and Rh: mass-transfer model

Because mass transfer can have significant effects on the

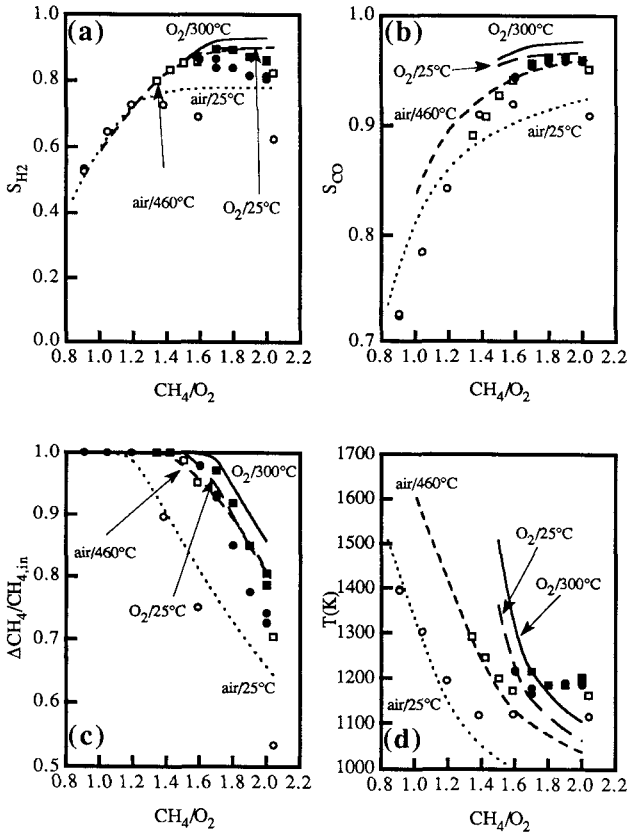

Figure 5. Experiments (symbols) and model (lines) (a) H_2 and (b) CO selectivities, (c) CH_4 conversions, and (d) surface temperatures for methane oxidation over an 80 ppi Rh foam monolith with 9.83 wt. % Pt.

Open symbols and dashed lines represent CH_4-air feeds, closed symbols and solid lines represent CH_4-O_2 feeds, circles represent feed temperatures of 25°C, and squares represent feeds preheated to 460°C (air) or 300°C (O_2).

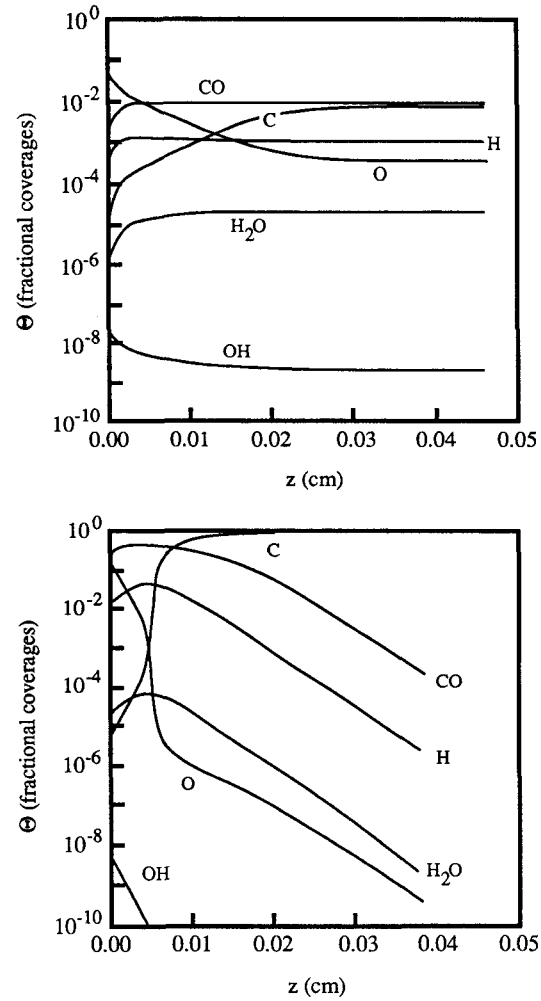

Figure 6. Fractional surface coverages as a function of axial position for PFR model simulations of room temperature feeds with (a) 15% CH_4 in air and (b) 30% CH_4 in air over a Rh catalyst.

selectivity of a partial oxidation reaction (Hickman and Schmidt, 1992b), the mass-transfer model was compared to the PFR model to determine the importance and the effect of boundary layer mass transfer for CH_4 oxidation over Pt and Rh monoliths. Figure 7 is a plot of the H_2 and CO selectivity and the axial length required for complete conversion of O_2 as a function of the mass-transfer coefficient k_c for a fixed feed composition (22.5% CH_4 in air) and a constant wall temperature (1,056 K) with the model parameters for Rh.

As shown, for $k_c > 1{,}000$ cm/s, the model predictions are independent of the mass-transfer coefficient. Similar results are observed at other feed compositions and temperatures for both the Rh and Pt model parameters. For lower values of k_c, the selectivities both increase slightly and the length required for complete conversion of oxygen increases dramatically. As shown in Figures 4 and 6, as the reaction proceeds, O_2 is consumed and the coverage of C increases. When all of the O_2 has been consumed, $\Theta_C \rightarrow 1$, and no more sites are available for additional reactions to occur. Thus, the lower values of k_c require longer residence times for complete conversion of O_2, allowing more time for H_2O to adsorb and provide additional O adatoms for the oxidation of carbon adatoms. Thus, the

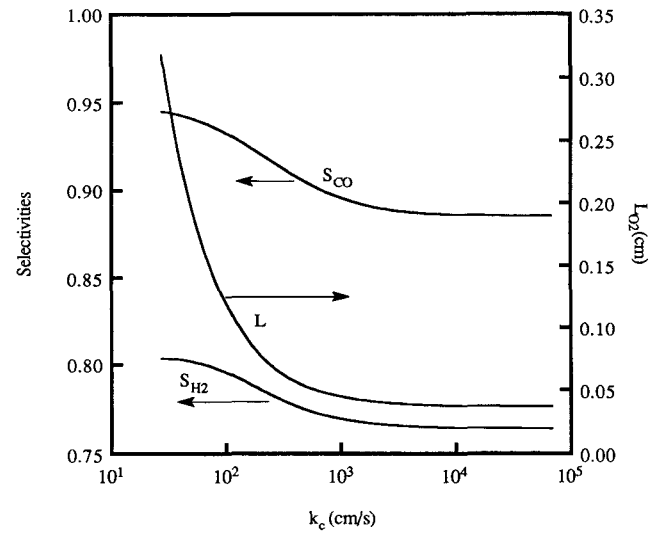

Figure 7. Variation with mass-transfer coefficient of the H_2 and CO selectivities and the axial length for complete conversion of O_2 (L_{O2}).

observed increases in S_{H2} and S_{CO} are primarily due to the increased residence time with available reaction sites. Essentially, more time is then available for the steam reforming reaction to occur:

$$CH_4 + H_2O \rightarrow CO + 3H_2. \quad (25)$$

This was confirmed with the model by showing that S_{H2} and S_{CO} change much less with k_c than shown in Figure 7 when H_2O adsorption is not allowed.

These results show that the PFR model is adequate for simulations of catalysts with geometries that give high rates of mass transfer (such as the foam monoliths in Figures 1 and 5). A mass-transfer coefficient of $\sim 10^2$ cm/s is estimated for laminar flow through cylindrical tubes with channel dimensions similar to those of the foam monoliths. By the Reynolds analogy, the mass-transfer coefficient is proportional to the friction factor for a fixed velocity (Cussler, 1984). Because the foam monoliths do not have straight channels, they have higher pressure drops than straight-channeled monoliths of similar channel dimensions and consequently will give even higher mass-transfer coefficients than estimated for flow in straight tubes. Thus, Figure 7 suggests that for foam monoliths with $k_c \sim 10^3$ cm/s, the exact value of the mass-transfer coefficient is not significant for these simulations. Even for k_c as low as 10^2 cm/s, the calculated selectivities only vary by less than 5%.

Typically, when an increase in the mass-transfer coefficient has no effect on the observed rates of conversion, the system is said to be "reaction-limited." However, in the case of these simulations for $k_c > 10^3$, *the observed rates are gas flux-limited.* Because the surface reaction rates are very fast, the overall rate is in fact primarily limited by the flux of reactant species ($r_{ads,i}$) to the catalyst surface. Although not shown here, increasing the value of the oxygen sticking coefficient (and thus k_{ao}) causes an inversely proportional decrease in L_{O2}, the reactor tube length required for complete conversion of O_2. Hence, for high rates of interphase mass transfer, these simulations show that CH_4 oxidation rates become O_2 flux-limited.

Discussion

Reaction rate parameters

One important objective of this effort was to determine whether the high-temperature oxidation of methane could be simulated by an elementary-step model. Obviously, the strength of this model is that it is based on reaction rate parameters from several *independent* studies of the various reaction steps. The data for the parameters are taken from studies of single crystal and polycrystalline catalyst studies and can be applied to this model because the monolith catalysts used in the atmospheric-pressure studies have high loadings of the noble metal which form large crystallites (Hickman and Schmidt, 1993) and are thus expected to behave similar to unsupported catalysts. The numerical values for these parameters are listed with their sources in Table 1. Unless otherwise mentioned in this section, all of the activation energies and preexponential factors were taken directly from the literature.

When more than one set of rate parameters (from experiments at low coverages) were reported in the literature for a given reaction step, the set that gave the best correlation with these CH_4 oxidation experiments was selected.

O-H Reactions. The reaction rate parameters for all of the steps involving only O and H adatoms (reactions 1-3, H, O and W) have been identified in two recent articles from this laboratory (Williams et al., 1992; Zum Mallen et al., 1993). According to these studies, the elementary steps in H_2 oxidation on Pt and Rh have been determined by fitting a model to experiments which measure the desorption of OH radicals by laser-induced fluorescence (LIF) over polycrystalline foils exposed to mixtures of H_2, O_2, and H_2O for surface temperatures above 1,000 K. In these studies, the adsorption of H_2 and O_2 was found to best-fit a first-order model. This first-order dependence is well established in the literature for O_2 (Yates et al., 1979; Monroe and Merrill, 1980) and for H_2 (Hellsing et al., 1987). First-order O_2 adsorption is assumed in many kinetic studies of CO oxidation and is consistent with a mechanism where the rate-controlling step involves the interaction of the adsorbing O_2 molecule with a single catalytic site (Oh et al., 1986).

All of the O-H reaction parameters were left unchanged from those published previously except for two slight modifications. As will be described in the section comparing model predictions to low-pressure CSTR experiments, the sticking coefficient for O_2 on Pt was decreased from 0.04 to 0.003 to better-fit the O_2 flux limit observed at high temperatures (Hasenberg, 1984). This value is not outside the range of other reported values in the literature (Kaul et al., 1987, and references therein). For Rh, the previously reported sticking coefficient of 0.01 was used (Oh et al., 1986). The second modification was the assignment of a nonzero rate for the dissociation of OH on Rh. This parameter was not important for the LIF experiments, and changing it to physically reasonable value of $k_{-1} = 10^{13} e^{-5,000/RT}$ had no significant effect on the atmospheric-pressure model results.

CO Adsorption/Desorption. Because of the importance of this reaction in the automobile catalytic converter, carbon monoxide oxidation kinetics on Pt and Rh have been studied extensively on both polycrystalline and single crystal samples, including a large number of experiments which measure the rates of CO adsorption and desorption. Thus, the adsorption and desorption rate parameters used in this modeling study were taken directly from the literature.

The desorption energy of carbon monoxide is approximately the same on both metals and has been shown to decrease as the CO coverage increases (McCabe and Schmidt, 1977; Thiel et al., 1979; Oh et al., 1986; Peterlinz et al., 1991). In the atmospheric-pressure simulations for Pt, the CO coverage was almost always less than 0.1, so a coverage-independent activation energy of 30 kcal/mol was used.

However, a coverage-dependent activation energy was used for CO on Rh. In previous modeling studies of carbon monoxide oxidation (Oh et al., 1986; Sant and Wolf, 1990), this coverage dependence has been approximated by a value that decreases linearly with CO coverage:

$$E_{dCO} = E_{dCO}(\Theta = 0) - \alpha_{CO}\Theta_{CO} \quad (26)$$

Since the Rh simulations gave CO coverages close to unity in some cases (Figure 6), a coverage-dependent activation energy for CO desorption was necessary to obtain good agreement between the model and experiments. These simulations used

the previously reported value of $\alpha_{CO} = 10.6$ kcal/mol (Sant and Wolf, 1990) with $E_{d CO} = 31.6$ at low coverages (Thiel et al., 1979).

CO + O Reaction. The bimolecular CO oxidation reaction has been studied extensively on various single-crystal and polycrystalline Pt surfaces, with reported activation energies ranging from 12 to 40 kcal/mol (Campbell et al., 1980; Gland and Kollin, 1983; Engstrom and Weinberg, 1988). This variation in activation energy is accompanied by a corresponding change in the preexponential and corresponds to different reaction conditions, with higher activation energies and preexponentials observed at low coverages and lower activation energies and preexponentials occurring with high oxygen coverages. For this study, a low coverage activation energy of 24 kcal/mol with a preexponential of 1×10^{15} (Campbell et al., 1980) was used, because oxygen coverages are expected (and calculated) to be low at the high temperatures and CH_4-rich conditions of these atmospheric pressure experiments. The preexponential factor was increased above the reported value of 1.1×10^{14} to obtain better agreement between model and experiments in both the low-pressure and high-pressure simulations.

Many of the discrepancies between the model and the low-pressure experiments are a result of the activation energy of the CO + O reaction. For example, at lower temperatures and lower CH_4/O_2 feed ratios, where O coverages are higher, the model predicts CO generation rates much lower than those experimentally observed (Figure 2). As described earlier, however, changing the rate parameters to those derived from experiments with high O coverages drastically improved the agreement between model and experiments in the high O coverage regime.

In kinetic studies of CO oxidation on Rh where CO is the dominant surface species, apparent activation energies of 20 to 33 kcal/mol were reported (Schwartz et al., 1986; Berlowitz, et al., 1988; Wong and McCabe, 1989; Oh et al., 1991a). However, the desorption of CO to free vacant sites for O_2 adsorption was the rate-limiting step in these experiments, so the observed activation energies are attributed to the desorption of CO, and determination of the CO + O reaction activation energy is less straightforward. An earlier study which modeled the kinetics of O_2 titration by CO (Campbell et al., 1979) found the CO + O surface reaction on polycrystalline Rh had two distinct activation energies: 14.3 kcal/mol for surface temperatures (T_s) below 529 K and 25.0 kcal/mol for $T_s > 529$ K. The higher activation energy, expected to apply in the low coverage limit, is consistent with a more recent molecular beam study of CO oxidation on Rh(111) (Brown and Sibener, 1988) and was used in these simulations.

In addition, the formation and desorption of CO_2 have been lumped into a single step for both metals. This assumption is consistent with the fact that CO_2 adsorbs dissociatively on these metals (Castner et al., 1978) and has been used in other elementary-step models of CO oxidation over Pt and Rh (Oh et al., 1986; Kaul et al., 1987; Sant and Wolf, 1990). Furthermore, the reverse reaction, the dissociative adsorption of CO_2, was not allowed in these modeling studies, since the CO_2 partial pressures were always very low and the residence times were very short. The effect of H_2O adsorption on Figure 7 shows that the adsorption of CO_2 should have no significant effect on the model predictions at these short residence times.

C + O Reaction. The C + O surface reaction has not been studied as extensively as the other C-O reactions, with most studies examining Ni catalysts and reporting activation energies from 32 to 43 kcal/mol (Astaldi et al., 1989; Kelemen and Krenos, 1985; Benziger and Preston, 1984). One recent study examined the reaction of O_2 with a carbon-covered Pt surface at 1,100 to 1,240 K and reported an activation energy of 46 kcal/mol for this reaction (Kislyuk et al., 1991). These experiments, however, were performed with polycrystalline Pt foils which were completely covered with carbon, and the results do not conclusively show that the C + O surface reaction is the rate-limiting step in these experiments.

The best fits to the data for the low-pressure experiments over Pt were obtained by choosing rate parameters with rates high enough so that the C + O reaction was not a rate-limiting step. Since the low-pressure results were independent of these rate parameters, they were chosen to best approximate the trends observed in the atmospheric-pressure experiments with Pt. Similar fits could be obtained with activation energies as high as the reported value of 46 kcal/mol as long as the preexponential factor was large enough ($\sim 10^{19}$ s^{-1}) to give the experimentally observed CH_4 conversion rates.

As discussed in the next section, making methane adsorption a single step in the model does not eliminate other adsorption mechanisms in which H atoms dissociate sequentially. Thus, the surface reaction mechanism may actually involve oxidation of an adsorbed CH_x species to form adsorbed CO and H. This is consistent with the following methane oxidation surface reaction sequence proposed by Oh et al. (1991b) for lower reaction temperatures on noble metals:

$$CH_x (x = 2 \text{ or } 3) + O \rightarrow HCHO \rightarrow CO + 2H \qquad (27)$$

Oh's mechanism is not inconsistent with the model, since (a) at higher temperatures, the conversion of CH_x to CO and H in reaction 27 may occur in a single concerted step, (b) Oh's mechanism does not allow for H abstraction by adsorbed O atoms,

$$CH_x + O \rightarrow CH_{x-1} + OH, \qquad (28)$$

and (c) the C + O reaction in this model is very fast. Since the C + O reaction is fast, the formation rate of adsorbed CO and H is controlled by the methane adsorption rate, and the model results do not change significantly if the model equations are modified so that some of the H atoms are removed from the adsorbed CH_x after the initial CH_4 chemisorption step.

The activation energy for the reverse reaction, CO dissociation, was calculated to be consistent with thermodynamic data for the gas-phase species at 298 K, with the assumption that C adsorbed on Pt is isenthalpic with graphitic carbon. This assumption essentially provides a lower bound for the activation energy of the CO dissociation reaction, since the binding energy for a carbon atom on a Pt surface [between 120 and 170 kcal/mol (Tully, 1980)] is equal to or less than the heat of sublimation of graphite (171 kcal/mol). The model was not very sensitive to the CO dissociation reaction rate parameters, since this rate was quite slow.

For the atmospheric-pressure simulations for Rh, the model predictions were much less sensitive to the rate parameters for both the forward and reverse reactions than for Pt (see Table

Table 3. Sensitivity Parameters*

Reaction		Pt 22.5% CH_4 in Air				Rh 20% CH_4 in Air			
		T(K)	S_{H2}	S_{CO}	$\frac{\Delta CH_4}{CH_{4in}}$	T(K)	S_{H2}	S_{CO}	$\frac{\Delta CH_4}{CH_{4in}}$
$H+O\rightarrow OH$	(1)	1.6	−19	5.7	−4.2	-1.1×10^{-1}	−5.5	7.8	-9.4×10^{-1}
$OH\rightarrow O+H$	(−1)	-5.5×10^{-4}	6.8×10^{-3}	-2.1×10^{-3}	1.5×10^{-3}	-2.5×10^{-4}	9.1×10^{-2}	-1.2×10^{-1}	1.8×10^{-2}
$H+OH\rightarrow H_2O$	(2)	6.2×10^{-4}	0.0	1.1×10^{-2}	0.0	3.1×10^{-4}	-9.2×10^{-2}	1.2×10^{-1}	-1.1×10^{-2}
$H_2O\rightarrow OH+H$	(−2)	-2.4×10^{-6}	2.8×10^{-5}	-1.2×10^{-5}	1.5×10^{-5}	-3.4×10^{-4}	6.5×10^{-4}	-3.4×10^{-4}	4.4×10^{-4}
$2OH\rightarrow H_2O+O$	(3)	-4.0×10^{-5}	5.1×10^{-3}	-3.0×10^{-3}	5.5×10^{-4}	0.0	0.0	0.0	0.0
$H_{2g}\rightarrow 2H$	(aH)	1.5	−18	5.3	−4.1	1.2×10^{-1}	−4.8	6.5	−1.0
$2H\rightarrow H_{2g}$	(dH)	−1.6	19	−5.8	4.2	-1.1×10^{-1}	5.8	−7.8	1.2
$O_{2g}\rightarrow 2O$	(aO)	5.3	−17	−11	−10	13	−8.2	−11	−14
$2O\rightarrow O_{2g}$	(dO)	-9.8×10^{-7}	0.0	0.0	0.0	-2.1×10^{-8}	0.0	0.0	0.0
$H_2O_g\rightarrow H_2O$	(aW)	3.8×10^{-5}	0.0	-1.3×10^{-4}	0.0	1.7×10^{-4}	0.0	-8.4×10^{-4}	0.0
$H_2O\rightarrow H_2O_g$	(dW)	-2.0×10^{-5}	2.5×10^{-4}	0.0	0.0	-9.2×10^{-5}	-1.3×10^{-4}	4.5×10^{-4}	1.1×10^{-4}
$C+O\rightarrow CO$	(4)	−2.2	11	2.1	4.6	-2.2×10^{-2}	2.2×10^{-2}	8.5×10^{-3}	2.6×10^{-2}
$CO\rightarrow C+O$	(−4)	3.6×10^{-2}	-2.0×10^{-1}	-1.1×10^{-2}	-8.2×10^{-2}	9.3×10^{-5}	-1.3×10^{-4}	0.0	-1.1×10^{-4}
$CH_{4g}\rightarrow C+4H$	(aM)	−5.3	17	11	10	−13	7.9	11	14
$CO+O\rightarrow CO_{2g}$	(dCD)	6.2×10^{-1}	8.1	−7.9	-3.3×10^{-1}	3.7×10^{-1}	5.6	−8.4	7.2×10^{-1}
$CO_g\rightarrow CO$	(aCM)	9.3×10^{-1}	6.5	−8.2	-9.8×10^{-1}	1.6	2.1	−5.6	−1.1
$CO\rightarrow CO_g$	(dCM)	-9.3×10^{-1}	−6.6	8.3	9.9×10^{-1}	−1.7	−2.3	6.0	1.2
α_{CO}						−1.7	−1.5	4.9	1.4

*As defined in Eq. 28, PFR model sensitivities (×100) to changes in the preexponential factors of various reaction steps (or change in the variable activation energy of CO desorption on Rh).

3). Since changing these parameters had little effect on the model results, the same values were used for Rh as for Pt, with the activation energy of the reverse reaction adjusted for thermodynamic consistency.

CH_4 Adsorption. For both Pt and Rh, the methane adsorption step was assumed to be first order in P_{CH4} and irreversible. Using higher-order kinetics had little effect generally on the model results. The assumption of irreversible adsorption was used, because the oxidation reactions are very fast, so little CH_4 would be expected to desorb under these reaction conditions.

Reaction (M) also lumps the breaking of all four C-H bonds into one step. Making this reaction a single step in the model does not eliminate other adsorption mechanisms in which H atoms dissociate sequentially, but it does eliminate the possibility of the abstraction of H atoms from adsorbed CH_x species by O adatoms, reaction 28. However, high selectivities for H_2 formation on Pt and Rh suggest that such abstraction reactions are not a dominant reaction step for CH_4-rich oxidation at high temperatures.

A final point is that CH_4 chemisorption was assumed to be activated, with Pt having a higher activation energy than Rh. The dissociative chemisorption of CH_4 on several different metal surfaces is a topic of much current research, with investigators using a variety of techniques to identify the important factors in CH_4 adsorption energetics. The value for Rh of 5 kcal/mol was taken from low-temperature studies of CH_4 adsorption on Rh films which estimate activation energies between 5 and 7 kcal/mol (Brass and Ehrlich, 1987; Stewart and Ehrlich, 1975). Similar experiments for polycrystalline Pt or Pt(111) have not been reported in the literature, although activation energies of 9.9 (Luntz and Bethune, 1989) and 14.4 (Sun and Weinberg, 1990) kcal/mol have been reported for other Pt crystal surfaces. The value of 10.3 kcal/mol was taken from a semiempirical electronic structure calculation for the activation energy of dissociative chemisorption on Pt(111) (Anderson and Maloney, 1988).

Parameter Sensitivities. An analysis of the sensitivity of the PFR model to slight changes in various rate parameters is tabulated in Table 3. These data were calculated by changing the preexponential factor for a given reaction step and calculating the resulting change in the selectivities, conversion and reactor temperature. The sensitivity of the model to a particular parameter is defined here as:

$$\text{sensitivity} = \frac{\Delta x/x}{\Delta k_i/k_{io}}, \tag{29}$$

where x is the model output variable of interest (T, S_{H2}, S_{CO}, or CH_4 conversion) and k_i is the parameter that is being varied (the reaction rate preexponentials). The data in Table 3 were calculated by making differential changes in a given parameter and determining the resulting change in the model output variables. For this analysis, the calculations for Pt and Rh were based on room temperature feeds of 20% and 22.5% CH_4 in air, respectively.

These data help to identify the reaction steps which play a significant role in determining the reaction selectivity. For example, the rate parameters for O_2 and CH_4 adsorption have the most profound impact on the model results. Changing one of these two adsorption rates essentially changes the stoichiometry of the available surface species, with higher O/fuel ratios giving lower partial oxidation selectivities. Since the available O_2 is always consumed, the reactant adsorption rates are the primary factors in determining the CH_4 conversion.

In addition, the adsorption and desorption rates of H_2 and CO have a significant impact on the model predictions. For example, a higher rate of adsorption or lower rate of desorption of H_2 increases the residence time of H on the surface, resulting in more H_2O and lower S_{H2}. Since the O/fuel ratio on the surface is determined primarily by the reactant adsorption rates, this decrease in S_{H2} is accompanied by an increase in S_{CO} because fewer O adatoms are available to oxidize CO before it desorbs.

Besides the adsorption and desorption steps, the (1) O + H, (4) C + O, and (*dCD*) CO + O surface reactions have the most significant effect on the catalyst selectivity. The relative rates of these reactions determine the partitioning of O between O-H reactions and O-C reactions. For instance, increasing the rate of reaction (Eq. 1) gives a higher rate of H_2O formation, decreasing S_{H2} and increasing S_{CO}. The sensitivity of the model to the parameters for the O + H reaction (Eq. 1) confirms that this reaction step is a key factor in making Rh more selective than Pt for the formation of H_2 during CH_4 oxidation.

An interesting difference between Pt and Rh is the sensitivity of the model to the parameters for the C + O reaction (Eq. 4). For Rh, the model is essentially insensitive to the parameters for both the forward and reverse reactions, while these parameters have a small effect on the model predictions for the Pt catalyst. This difference may be due to the different O coverages on the two metals, with the lower O coverages on Pt making this step a small, but significant, factor in determining product selectivities.

Comparison of Pt and Rh. Based on the activation energies used in these models, potential energy diagrams for CH_4 oxidation in the low coverage limit are shown in Figures 8 and 9. To present the various surface reactions in a single, coherent diagram, a CH_4/O_2 stoichiometry of 1/2 was used. Thus, all of the activation energies for the O-H reactions on the right half have been multiplied by a factor of 2 to account for this stoichiometry. In addition, the secondary (less significant) O-H reaction path represented by reaction 3 has been excluded to simplify the diagram.

By comparing these potential energy "landscapes," one can get a better understanding of the causes behind the differences between Pt and Rh. A comparison of the left sides of the diagrams shows a strong similarity between Rh and Pt for the C-O reactions, with the primary difference being the activation energy of CH_4 chemisorption. The right sides, however, are strikingly different with respect to the formation of OH from O and H. The formation of OH requires crossing a significant energy barrier on Rh but is relatively unhindered on Pt. The drastically different catalytic selectivities of Rh and Pt are attributed to this difference.

Role of mass transfer

The model results for the mass-transfer model show that for high rates of mass transfer, these reactions become flux-limited. This result may explain why in earlier experiments with both extruded (straight-channeled) and foam monoliths coated with Pt (Hickman and Schmidt, 1992b), similar product selectivities and conversions were observed for both geometries. In an earlier article (Hickman and Schmidt, 1992c), it was shown that the effect of mass transfer on selectivity depends on the reaction orders of the partial and total oxidation steps. A partial oxidation reaction can be described by the following series-parallel reaction scheme:

$$A \rightarrow B,\ r_1 = k_1 c_{As}^{m_{1A}} \tag{30}$$

$$A + B \rightarrow 2C,\ r_2 = k_2 c_{As}^{m_{2A}} c_{Bs}^{m_{2B}} \tag{31}$$

$$\frac{dc_B}{dc_c} = \frac{k_1 c_{As}^{(m_{1A} - m_{2A})}}{2k_2 c_{Bs}^{m_{2B}}} - \frac{1}{2} \tag{32}$$

As shown in Eq. 32, changes in the mass-transfer coefficient have the greatest effect on reaction selectivity when $m_{1A} \neq m_{2A}$. Although the CH_4 oxidation model in this article is much more complex than this simplified scheme, the observed relative

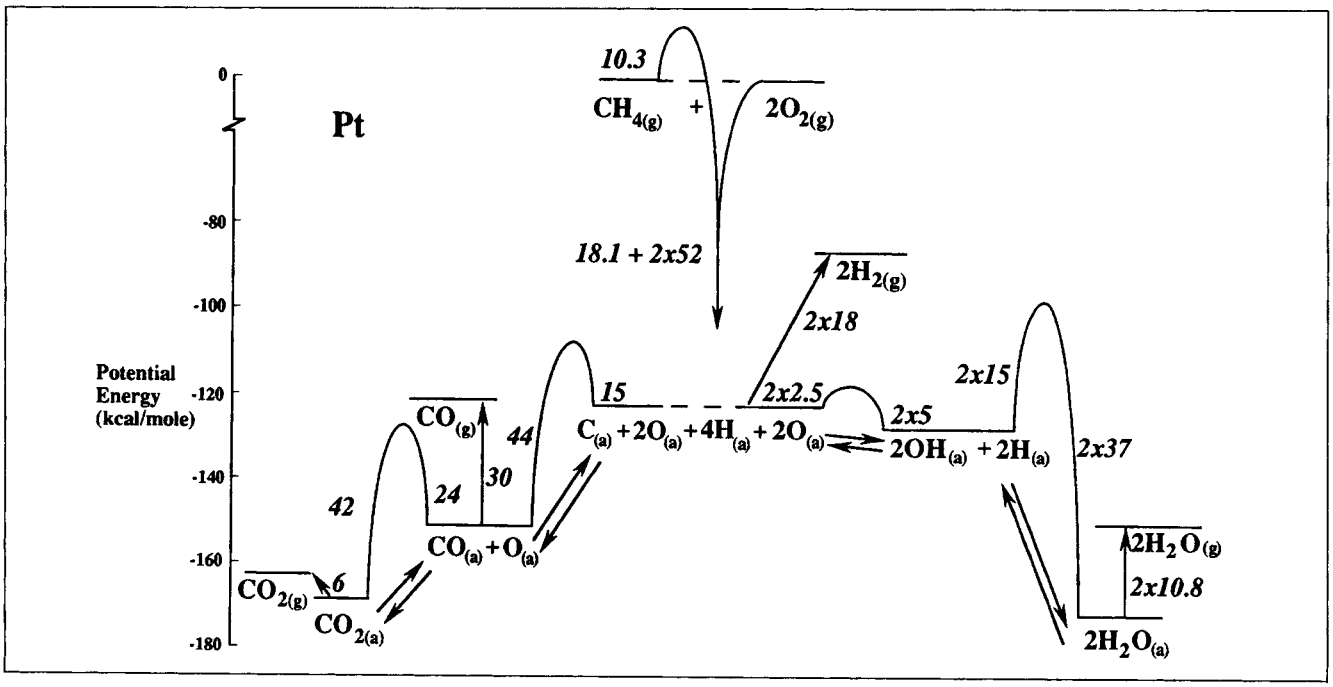

Figure 8. Potential energy for the CH_4 oxidation reaction system at low coverages on Pt.

The potential energy values (*y*-axis) are calculated relative to CH_{4g} and O_{2g} at 298 K. Gas-phase species are denoted by the subscript *g*; all other species are surface species.

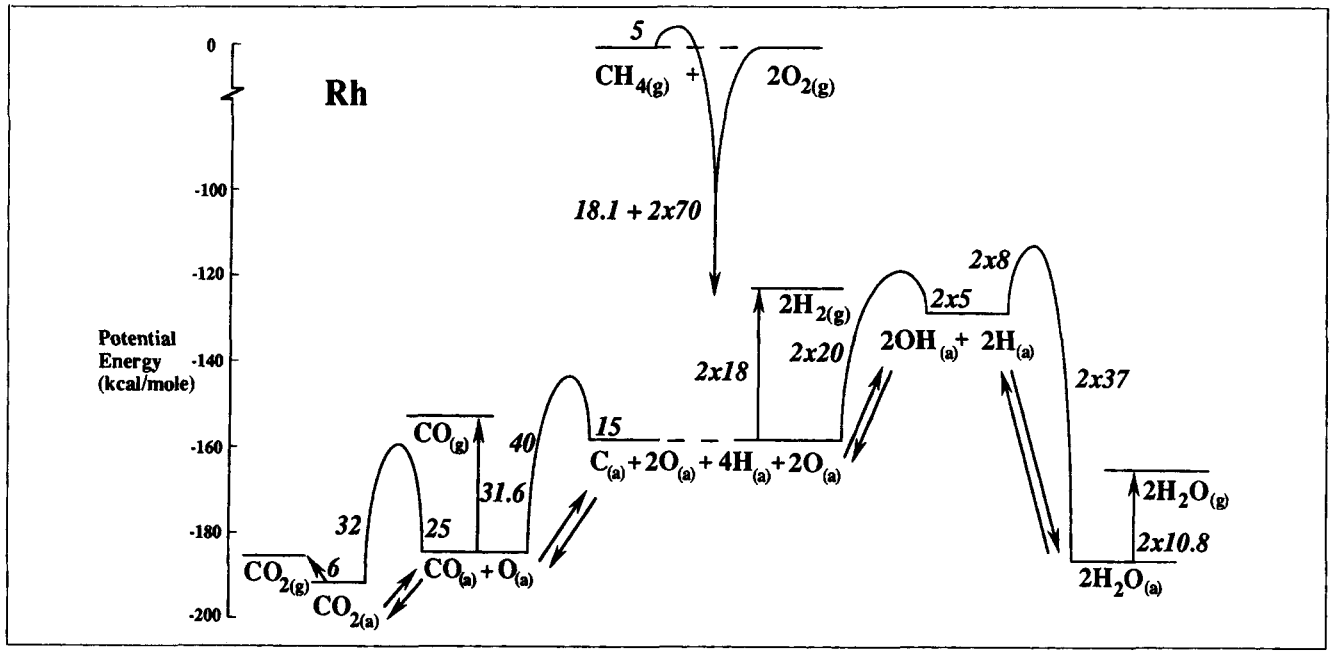

Figure 9. Potential energy for the CH_4 oxidation reaction system at low coverages on Rh.

The potential energy values (y-axis) are calculated relative to CH_{4g} and O_{2g} at 298 K. Gas-phase species are denoted by the subscript g; all other species are surface species.

insignificance of the mass-transfer coefficient is largely due to the fact that the partial oxidation and total oxidation steps have effectively the same reaction order with respect to O_2.

Applicability of the model

As with any model of a reaction system, one must consider the assumptions made in developing the model when evaluating the results. The primary feature of this model is the use of reaction rate parameters derived from experiments over model catalysts in the low coverage limit. This feature limits applicability of this model to high temperature conditions with catalysts where metal-support interactions are not significant. The high temperatures ensure low coverages, and the absence of significant metal-support interactions is important when using rate parameters from experiments over polycrystalline and single-crystal catalysts.

In the atmospheric-pressure experiments described earlier, the monolith catalysts were coated with very high loadings (~10%) of Pt or Rh. These catalysts were shown previously to consist of large metal crystallites of the noble metal on the monolith surface (Hickman and Schmidt, 1993). Thus, the alumina support is expected to have little or no effect, and the observed catalytic activity should be due solely to the noble metal. This feature, combined with the high autothermal temperatures encountered during methane oxidation, makes these catalysts ideal candidates for a model based on catalytic reaction rate studies at low coverages.

Beside being limited to low coverage situations, the reliability of the model may depend on the microstructure of the catalyst and the structure sensitivity of the surface reactions. The model essentially assumes that the rate parameters used are adequate approximations of the average behavior observed over a real catalyst where many different crystal faces and surface defects are exposed. The good agreement between the model predictions and experimental results is strong evidence that this "surface averaging" is a good approximation and is consistent with many previous studies of CO oxidation which show that this reaction is essentially insensitive to the catalyst microstructure.

The surprisingly good accuracy of this model has important implications for use of this and similar models in catalyst and reactor design. The comparison of Pt and Rh outlined earlier is a good example of the application of such a model to catalyst design. Because the model is based on an elementary-step reaction scheme, differences in catalytic selectivity during CH_4 oxidation over Pt and Rh are *predicted* to occur because of the variations in the energetics of individual reaction steps. As reaction data are accumulated for other reaction steps and other catalyst surfaces, a library of data (such as is found in the combustion literature for gas-phase reactions) will allow for more detailed models to be developed.

In addition, catalytic reactor models generally implement empirical rate expressions which have limited usefulness outside of the range of conditions under which they were derived. The use of elementary-step models based on the reaction mechanism allows more reliable extrapolations to be made. As demonstrated, rate parameters from low-pressure studies can be extrapolated to high-pressure CH_4 oxidation experiments within the limits of the low coverage conditions under which the rate parameters were measured.

Summary

An elementary-step model of CH_4 oxidation has been developed using rate parameters from the literature. This model has been shown to agree with data from low-pressure experiments over polycrystalline Pt catalysts. In addition, this model also predicts selectivities and conversions similar to those ob-

served at the atmospheric-pressure conditions used in a laboratory-scale methane to synthesis gas reactor which contains monolith catalysts coated with high loadings of Pt and Rh.

For catalysts which give high interphase mass-transfer rates, such as the foam monoliths used in the atmospheric-pressure experiments, a plug flow tubular reactor model adequately describes all experimental results, because the reactions are actually flux-limited rather than mass-transfer-limited.

The consistency of the model and experimental results strongly suggests that, under CH_4-rich conditions at high temperatures, H_2 and CO are primary products of the direct oxidation of methane via a pyrolysis mechanism. Based on rate parameters from experiments at low coverages, this model demonstrates that the superiority of Rh over Pt for the direct oxidation of CH_4 to H_2 and CO is due primarily to the difference in the activation energy for formation of OH from O and H adatoms (20 kcal/mol for Rh vs 2.5 kcal/mol for Pt).

Acknowledgment

This research was supported partially by DOE under Grant No. DE-FG02-88ER13878-A02.

Notation

A = cross-sectional area of flow
A_{surf} = catalyst surface area
c_i = bulk molar concentration of species i in the gas phase
c_{is} = molar concentration of species i in the gas phase at the surface
E_i = activation energy of reaction i
k_i = rate coefficient for reaction i (units shown are for first order)
m_{ji} = order of reaction j with respect to component i
M_i = molecular weight of species i
F = total molar flow rate
F_i = molar flow rate of species i (subscript o implies inlet flow rate)
F_o = total molar flow rate at tube inlet
L_{O2} = reaction tube length required for complete conversion of O_2
N_{av} = Avogadro's number
N_o = monolayer coverage (assumed to be 10^{15} molec./cm^2)
P = reactor pressure
P_{bi} = partial pressure of i in the bulk gas phase
P_i = partial pressure of species i at the catalyst surface
$P_{i,o}$ = feed partial pressure of component i
r_i = net flux of species i from the catalyst surface ($r_{des,i} - r_{ads,i}$)
R_g = gas constant
s_i = sticking coefficient of species i
S_{H2} = selectivity of formation of H_2, (defined in Eq. 23)
S_{CO} = selectivity of formation of CO, (defined in Eq. 24)
T_g = gas temperature
T_o = initial (feed) temperature
T_s = autothermal surface temperature
$(UA)_{loss}$ = overall heat-transfer coefficient representing heat lost through reactor walls
v_o = velocity air tube inlet
V_R = reactor volume

Greek letters

Θ_i = fractional surface coverage of species i (v = vacant sites)
$\Theta_{v,NC}$ = fractional coverage of available vacant noncompetitive surface sites
ρ_o = density at tube inlet
σ = tube perimeter
τ = reactor residence time (assumed identical for all species)

Literature Cited

Anderson, A. B., and J. J. Maloney, "Activation of Methane on Iron, Nickel, and Platinum Surfaces: A Molecular Orbital Study," *J. Phys. Chem.*, **92**, 809 (1988).

Astaldi, C., A. Santoni, F. Della Valle, and R. Rosei, "CO Dissociation and Recombination Reactions on Ni(100)," *Surf. Sci.*, **220**, 322 (1989).

Benziger, J. B., and R. E. Preston, "Recombination Reactions on Ni(111)," *Surf. Sci.*, **141**, 567 (1984).

Berlowitz, P. J., C. H. F. Peden, and D. W. Goodman, "Kinetics of CO Oxidation on Single-Crystal Pd, Pt, and Ir," *J. Phys. Chem.*, **92**, 5213 (1988).

Brass, S. G., and G. Ehrlich, "Internal Molecular Motions and Activated Chemisorption: CH_4 on Rhodium," *J. Chem. Phys.*, **87**(8), 4285 (1987).

Brown, L. S., and S. J. Sibener, "A Molecular Beam Scattering Investigation of the Oxidation of Carbon Monoxide on Rh(111): I. Kinetics and Mechanism," *J. Chem. Phys.*, **89**(2), 1163 (1988).

Campbell, C. T., S.-K. Shi, and J. M. White, "Kinetics of Oxygen Titration by Carbon Monoxide on Rhodium," *J. Phys. Chem.*, **83**(17), 2255 (1979).

Campbell, C. T., G. Ertl, H. Kuipers, and J. Segner, "A Molecular Beam Study of the Catalytic Oxidation of Carbon Monoxide on a Pt(111) Surface," *J. Chem. Phys.*, **73**, 5862 (1980).

Campbell, C. T., G. Ertl, H. Kuipers, and J. Segner, "A Molecular Beam Investigation of the Interactions of CO with a Pt(111) Surface," *Surf. Sci.*, **107**, 207 (1981).

Castner, D. G., B. A. Sexton, and G. A. Somorjai, "LEED and Thermal Desorption Studies of Small Molecules (H_2, O_2, CO, CO_2, NO, C_2H_4, C_2H_6, and C) Chemisorbed on the Rhodium (111) and (100) Surfaces," *Surf. Sci.*, **71**, 519 (1978).

Cussler, E. L., *Diffusion: Mass Transfer in Fluid Systems*, Cambridge Univ. Press, New York (1984).

Engstrom, J. R., and W. H. Weinberg, "Analysis of Gas-Surface Reactions by Surface Temperature Modulation: Experimental Applications to the Adsorption and Oxidation of CO on the Pt(110)-(1×2) Surface," *Surf. Sci.*, **201**, 145 (1988).

Fisher, G. B., and J. L. Gland, "The Interaction of Water with the Pt(111) Surface," *Surf. Sci.*, **94**, 446 (1977).

Gear, C. W., *Numerical Initial Value Problems in Ordinary Differential Equations*, Prentice-Hall, Englewood Cliffs, NJ (1971).

Gland, J. L., and E. B. Kollin, "Carbon Monoxide Oxidation on the Pt(111) Surface: Temperature Programmed Reaction of Coadsorbed Atomic Oxygen and Carbon Monoxide," *J. Chem. Phys.*, **78**(2), 963 (1983).

Hasenberg, D., "HCN Synthesis on Polycrystalline Platinum and Rhodium," PhD Thesis, Univ. of Minnesota (1984).

Heck, R. H., J. Wei, and J. R. Katzer, "Mathematical Modeling of Monolithic Catalysts," *AIChE J.*, **22**(3), 477 (1976).

Hellsing, B., B. Kasemo, S. Ljungström, A. Rosén, and T. Wahnström, "Kinetic Model and Experimental Results for H_2O and OH Production Rates on Pt," *Surf. Sci.*, **189/190**, 851 (1987).

Hickman, D. A., E. A. Haupfear, and L. D. Schmidt, "Synthesis Gas Formation by Direct Oxidation of Methane over Rh Monoliths," *Catal. Lett.*, **17**, 223 (1993).

Hickman, D. A., and L. D. Schmidt, "Synthesis Gas Formation by Direct Oxidation of Methane over Pt Monoliths," *J. Catal.*, **138**, 267 (1992a).

Hickman, D. A., and L. D. Schmidt, "The Role of Boundary Layer Mass Transfer in Partial Oxidation Selectivity," *J. Catal.*, **136**, 300 (1992b).

Kaul, D. J., R. Sant, and E. E. Wolf, "Elementary-Step Modeling and Transient FTIR Studies of CO Oxidation on Pt/SiO_2," *Chem. Eng. Sci.*, **42**(6), 1399 (1987).

Kelemen, S. R., and J. Krenos, "Oxidation Studies of Carbided Nickel Surfaces," *Surf. Sci.*, **157**, 491 (1985).

Kislyuk, M. U., V. V. Migulin, V. V. Savkin, A. G. Vlasenko, A. V. Sklyarov, and I. Tret'yakov, "Reaction of Oxygen with Carbon on a Platinum Surface and the Spatial Distribution of the Carbon Monoxide Produced," *Kinet. Catal.*, **31**(6), 1219 (1991).

Kiss, J., and F. Solymosi, "Adsorption of H_2O on Clean and Boron-Contaminated Rh Surfaces," *Surf. Sci.*, **177**, 191 (1986).

Luntz, A. C., and D. S. Bethune, "Activation of Methane Dissociation on a Pt(111) Surface," *J. Chem. Phys.*, **90**(2), 1274 (1989).

Marks, C. M., and L. D. Schmidt, "Hydroxyl Radical Desorption in Catalytic Combustion," *Chem. Phys. Lett.*, **178**(4), 358 (1991).

Matsushima, T., "Dissociation of Oxygen Admolecules on Rh(111), Pt(111), and Pd(111) Surfaces at Low Temperatures," *Surf. Sci.*, **157**, 297 (1985).

McCabe, R. W., and L. D. Schmidt, "Binding States of CO and H_2 on Clean and Oxidized Pt(111)," *Surf. Sci.*, **65**, 189 (1977).

Oh, S. H., G. B. Fisher, J. E. Carpenter, and D. W. Goodman, "Comparative Kinetic Studies of CO-O_2 and CO-NO Reactions over Single Crystal and Supported Rhodium Catalysts," *J. Catal.*, **100**, 360 (1986).

Oh, S. H., and C. C Eickel, "Influence of Metal Particle Size and Support on the Catalytic Properties of Supported Rhodium: CO-O_2 and CO-NO Reaction," *J. Catal.*, **128**, 526 (1991a).

Oh, S. H., P. J. Mitchell, and R. M. Siewert, "Methane Oxidation over Alumina-Supported Noble Metal Catalysts with and without Cerium Additives," *J. Catal.*, **132**, 287 (1991b).

Peterlinz, K. A., T. J. Curtiss, and S. J. Sibener, "Coverage Dependent Desorption Kinetics of CO from Rh(111) Using Time Resolved Specular Helium Scattering," *J. Chem. Phys.*, **95**, 6972 (1991).

Root, T. W., L. D. Schmidt, and G. B. Fisher, "Adsorption and Reaction of Nitric Oxide and Oxygen on Rh(111)," *Surf. Sci.*, **134**, 30 (1983).

Sant, R., and E. E. Wolf, "Elementary-Step Modeling and Transient FTIR Studies of CO Oxidation on Rh/SiO_2," *Chem. Eng. Sci.*, **45**(10), 3137 (1990).

Schwartz, S. B., L. D. Schmidt, and G. B. Fisher, "CO + O_2 Reaction on Rh(111): Steady-State Rates and Adsorbate Coverages," *J. Phys. Chem.*, **90**, 6194 (1986).

Stewart, C. N., and G. Ehrlich, "Dynamics of Activated Chemisorption: Methane on Rhodium," *J. Chem. Phys.*, **62**(12), 4672 (1975).

Sun, Y.-K., and W. H. Weinberg, "Kinetics of Dissociative Chemisorption of Methane and Ethane on Pt(110)-(1 × 2)," *J. Vac. Sci. Technol. A*, **8**(3), 2445 (1990).

Thiel, P. A., E. D. Williams, J. T. Yates, Jr., and W. H. Weinberg, "Interaction of Oxygen with the Rh(111) Surface," *Surf. Sci.*, **84**, 54 (1979).

Tully, J. C., "Dynamics of Gas-Surface Interactions: Reaction of Atomic Oxygen with Adsorbed Carbon on Platinum," *J. Chem. Phys.*, **73**, 6333 (1980).

Votruba, J., J. Sinkule, V. Hlavácek, and J. Skrivánek, "Heat and Mass Transfer in Monolithic Honeycomb Catalysts," *Chem. Eng. Sci.*, **30**, 117 (1975).

Wagner, F. T., and T. E. Moylan, "A Comparison Between Water Adsorbed on Rh(111) and Pt(111), With and Without Predosed Oxygen," *Surf. Sci.*, **191**, 121 (1987).

Wagner, M. L., and L. D. Schmidt, "Model Oxidation Reactions: The Coadsorption of O_2 with H_2, NH_3, and N_2H_4 on Rh(111)," *J. Phys. Chem.*, in press (1993).

Williams, W. R., C. M. Marks, and L. D. Schmidt, "Steps in the Reaction $H_2 + O_2 \leftrightarrow H_2O$ on Pt: OH Desorption at High Temperatures," *J. Phys. Chem.*, **96**, 5922 (1992).

Wong, C., and R. W. McCabe, "Effects of High Temperature Oxidation and Reduction on the Structure and Activity of Rh/Al_2O_3 and Rh/SiO_2 Catalysts," *J. Catal.*, **119**, 47 (1989).

Yates, J. T., P. A. Thiel, and W. H. Weinberg, "The Catalytic Reaction Between Adsorbed Oxygen and Adsorbed Hydrogen on Rh(111)," *Surf. Sci.*, **82**, 45 (1979).

Young, L. C., and B. A. Finlayson, "Mathematical Models of the Monolith Catalytic Converter: Part I. Development of Model and Application of Orthogonal Collocation," *AIChE J.*, **22**(2), 331 (1976).

Zum Mallen, M. P., W. R. Williams, and L. D. Schmidt, "Steps in H_2 Oxidation on Rh: OH Desorption at High Temperatures," *J. Phys. Chem.*, **97**, 625 (1993).

Manuscript received Aug. 24, 1992, and revision received Dec. 16, 1992.